European Journal of Mechanics B/Fluids 28 (2009) 590–598

Contents lists available at ScienceDirect

European Journal of Mechanics B/Fluids

www.elsevier.com/locate/ejmflu

A numerical study of mixed convection in a horizontal channel with a discrete heat source in an open cavity

Saiied M. Aminossadati [a,*], Behzad Ghasemi [b]

[a] School of Engineering, The University of Queensland, CRCMining, Brisbane, Australia
[b] Engineering Faculty, Shahrekord University, Shahrekord, P.O. Box 115, Iran

ARTICLE INFO

Article history:
Received 4 December 2007
Received in revised form 27 November 2008
Accepted 16 January 2009
Available online 21 January 2009

Keywords:
Mixed convection
Channel
Open cavity
Aspect ratio
Richardson number

ABSTRACT

This article aims to numerically investigate mixed convection heat transfer in a two-dimensional horizontal channel with an open cavity. A discrete heat source is considered to be located on one of the walls of the cavity. Three different heating modes are considered which relate to the location of the heat source on three different walls (left, right and bottom) of the cavity. The analysis is carried out for a range of Richardson numbers and cavity aspect ratios. The results show that there are noticeable differences among the three heating modes. When the heat source is located on the right wall, the cavity with an aspect ratio of two has the highest heat transfer rate compared to other cavity heating modes. Moreover, when the heat source is located on the bottom wall, the flow field in the cavity with an aspect ratio of two experiences a fluctuating behaviour for Richardson number of 10. The results also show that at a fixed value of Richardson number, all three different heating modes show noticeable improvements in the heat transfer mechanism as the cavity aspect ratio increases.

1. Introduction

In integrated electronic circuit boards with increasing package density, an effective heat removal process is required to ensure satisfactory operation of high heat generating components. Numerous innovative heat transfer strategies have been proposed and the fluid flow and heat transfer characteristics of such strategies have been experimentally and numerically investigated as detailed by Incropera [1] and Peterson and Ortega [2]. In the past few decades, mixed convection heat transfer has been a great interest for many engineering and science researchers in the electronic industry. The main objective of their studies has been to understand the fundamentals of various cooling strategies and to achieve a high performance cooling method which meets the heat removal needs of electronic devices with certain geometries.

Some researchers used open channels to simulate the mixed convection heat transfer in electronic devices [3–6]. Channels with open top upright cavities have also been used by some researchers to simulate the heat transfer mechanism for either pure natural convection [7–11] or mixed convection [12–14]. Manca et al. [15] presented a numerical study on mixed convection in an open cavity with a heated wall bounded by horizontally insulated plate. They considered three basic heating modes for the open cavity (assisting flow, opposing flow and heating from below) and compared their thermal performances. Brown and Lai [16] numerically studied a horizontal channel with an open cavity and obtained correlations for combined heat and mass transfer which covered the entire convection regime from natural, mixed, to forced convection. Leong et al. [17] studied the mixed convection for the same geometry used by Brown and Lai [16], showing that Reynolds number and Grashof number controlled the flow pattern and the transition to the mixed convection regime. They argued that in the mixed convection regime, the flow field might have become unstable. Manca et al. [18] presented an experimental investigation on the mixed convection in a channel with open cavity having a heated wall on the inflow side. They analysed the flow and temperature patterns for different Reynolds numbers and showed that the average temperature within the cavity varied with Reynolds number.

It is clear that the mixed convection heat transfer in enclosures and channels has received great interest in recent years. However, to the best knowledge of the authors, mixed convection in a channel with an open cavity having a localised heat source has received little attention in the literature. It is expected that the location of the heat source in the cavity significantly affects the interaction between the forced flow in the channel and the natural convection flow generated in the cavity [15,19,20]. A proposed heat management strategy should aim to achieve a high cooling effectiveness by considering the overall heat dissipation and taking into account the interaction between natural and forced convection flows. As such, the objective of this research is to study the mixed convection heat transfer in a two-dimensional horizontal channel with an open cavity with the emphasis on the effects of placement of the

* Corresponding author. Tel.: +61 7 33653676; fax: +61 7 33653888.
E-mail address: uqsamino@uq.edu.au (S.M. Aminossadati).

0997-7546/$ – see front matter
doi:10.1016/j.euromechflu.2009.01.001

Nomenclature

g	gravity
Gr	Grashof number, $g\beta H^3(T_H - T_C)/\nu^2$
H	height of the channel (Fig. 1)
H	depth of the cavity (Fig. 1)
K	conduction coefficient
L	width of the cavity
Le	exit length of the channel
N	normal vector to the surface
Nu	Nusselt number, $Nu = -(\partial\theta/\partial N)_s$
Nu_m	average Nusselt number
p	pressure
P	dimensionless pressure, $\bar{p}/\rho u_i^2$
$\bar{p}$	modified pressure, $p + \rho_i g y$
Pr	Prandtl number, ν/α
Re	Reynolds number, $u_i H/\nu$
Ri	Richardson number, $Ri = Gr/Re^2$
t	time
T	temperature
T_C	inlet flow temperature
T_H	heat source temperature
u_i	inlet flow velocity
u	x component of velocity
U	dimensionless form of u (u/u_i)
v	y component of velocity
V	dimensionless form of v (v/u_i)
x, y	coordinates
X, Y	dimensionless coordinates, x/H, y/H

Greek symbols

α	heat diffusivity coefficient
β	fluid volume expansion coefficient
θ	dimensionless temp. $(T - T_c)/(T_H - T_C)$
θ_{fm}	average dimensionless temperature
μ	fluid viscosity
ν	kinematic fluid viscosity
ρ	density
ψ	stream function
τ	dimensionless time, $u_i t/H$

Subscripts

max	maximum
min	minimum

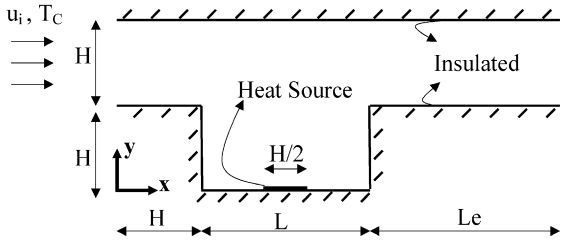

Fig. 1. A schematic diagram of the channel.

localised heat source in the cavity and the aspect ratio of the cavity. This leads to an appropriate design of the placement of high heat generating electronic components which, in turn, results in a superior cooling performance for the electronic device.

2. Problem definition

The geometry considered in this study is a two-dimensional horizontal channel with an open cavity (Fig. 1). Air is introduced to the channel at a uniform velocity, u_i, and temperature, T_C. The air flow is assumed to be laminar and incompressible with the Prandtl number of $Pr = 0.71$. The walls of the channel and the cavity are insulated. The height of the inflow and outflow openings is equal to the depth of the cavity. Three heating modes are considered which relate to the location of a discrete heat source on one of the three different walls (left, right or bottom) of the cavity (Fig. 2). The width and height of the heat source are $H/2$ and $H/20$, respectively.

Throughout the analysis, Grashof number is assumed constant ($Gr = 10^4$) and Richardson number has been varied ($0.01 \leqslant Ri \leqslant 100$). Since Richardson number is related to Reynolds number ($Ri = Gr/Re^2$), increasing Richardson number at a fixed Grashof number is associated with decreasing Reynolds number. This means lowering the strength of externally induced air flow or increasing the effect of buoyancy forces in the flow field. In the first part of this study, the cavity aspect ratio is assumed constant ($L/H = 2$) and the three heating modes are analysed for different Richardson numbers ($0.01 \leqslant Ri \leqslant 100$). In the second part, the cavity aspect

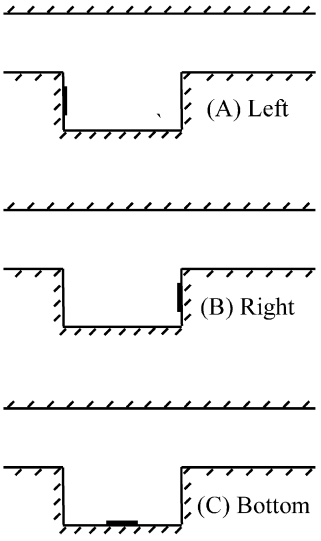

Fig. 2. Three different locations of the heat source in the cavity.

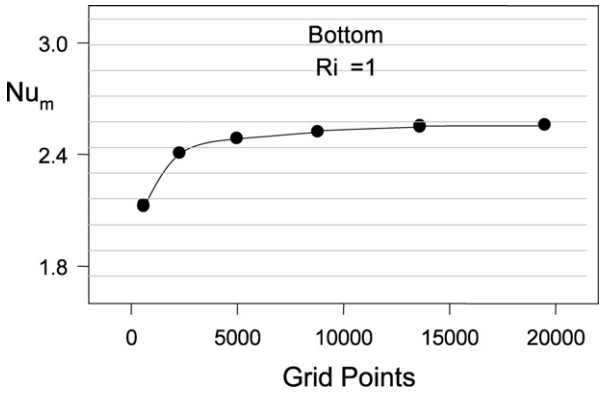

Fig. 3. The effect of grid refinement on the average Nusselt number. Heat source is located on the bottom wall of the cavity, $L/H = 2$, and $Le/H = 2$.

Table 1
A comparison between the present study and Manca et al. [15] for case (left, $H/D = 1$, $Re = 100$).

Richardson number	Maximum fluid temperature			Minimum stream function		
	θ_{max} [15]	θ_{max} [present]	Difference (%)	ψ_{min} [15]	ψ_{min} [present]	Difference (%)
0.01	0.576	0.577	0.2	−0.0600	−0.0600	0
0.1	0.544	0.545	0.2	−0.0640	−0.0640	0
1	0.420	0.422	0.5	−0.0899	−0.0900	0.1
10	0.303	0.305	0.7	−0.1950	−0.1940	0.5
100	0.209	0.211	1.0	−0.4320	−0.4240	1.9

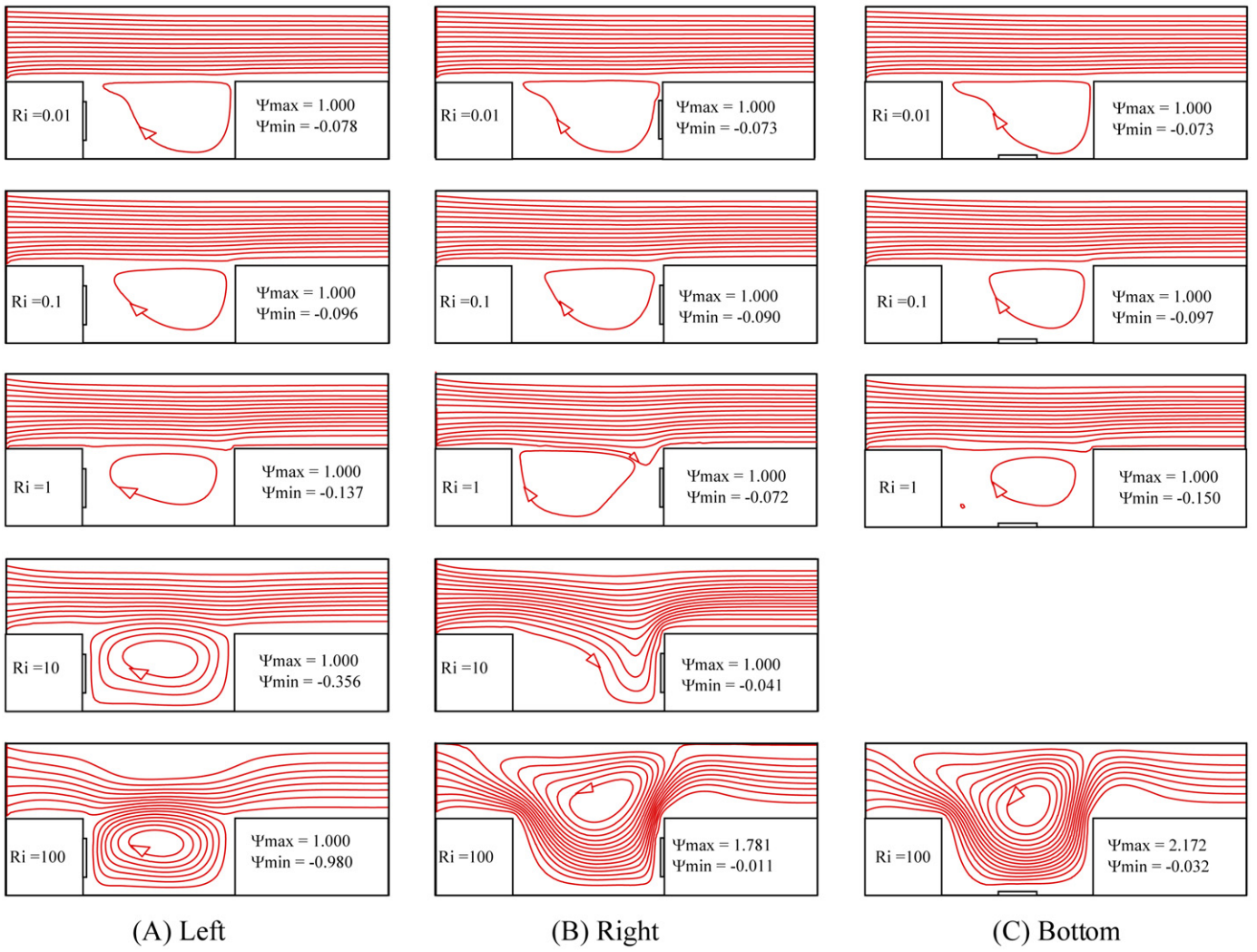

Fig. 4. The flow patterns for different locations of the heat source and various Richardson numbers.

ratio is varied ($0.5 \leqslant L/H \leqslant 5$) so that the effects of the dimension of the cavity on the channel thermal performance can be studied.

3. Governing equations

The governing equations for a domain within a two-dimensional channel with an open cavity, which includes the fluid and the heat source, are presented below. The governing equations in non-dimensional forms are as follows:

$$\frac{\partial U}{\partial X} + \frac{\partial V}{\partial Y} = 0, \tag{1}$$

$$\frac{\partial U}{\partial \tau} + U\frac{\partial U}{\partial X} + V\frac{\partial U}{\partial Y} = -\frac{\partial P}{\partial X} + \frac{1}{Re}\left(\frac{\partial^2 U}{\partial X^2} + \frac{\partial^2 U}{\partial Y^2}\right), \tag{2}$$

$$\frac{\partial V}{\partial \tau} + U\frac{\partial V}{\partial X} + V\frac{\partial V}{\partial Y} = -\frac{\partial P}{\partial Y} + \frac{1}{Re}\left(\frac{\partial^2 V}{\partial X^2} + \frac{\partial^2 V}{\partial Y^2}\right) + \frac{Gr}{Re^2}\theta, \tag{3}$$

$$\frac{\partial \theta}{\partial \tau} + U\frac{\partial \theta}{\partial X} + V\frac{\partial \theta}{\partial Y} = \frac{1}{Pr\,Re}\left(\frac{\partial^2 \theta}{\partial X^2} + \frac{\partial^2 \theta}{\partial Y^2}\right), \tag{4}$$

where, τ is the time in a dimensionless form ($\tau = u_i t/H$) and all the lengths are normalised by the depth of the cavity ($X = x/H$, $Y = y/H$). Velocities are normalised by the inlet velocity ($U = u/u_i$, $V = v/u_i$). The pressure is normalised as $P = \bar{p}/\rho u_i^2$, where $\bar{p}$ is the modified pressure ($p = p + \rho_C g y$). The non-dimensional form of temperature is $\theta = (T - T_C)/(T_H - T_C)$. All the thermo-physical properties of the air flow are assumed constant except for the variation in density with temperature, where a Boussinesq approximation is applied. Fully-developed conditions are considered at the exit section of the channel and no-slip boundary conditions ($U = V = 0$) are assumed on all the walls. Velocities at the entry section are $V = 0$, $U = 1$ and at the exit section are $V = 0$, $\partial U/\partial X = 0$. In addition, at the entry section, the temperature is

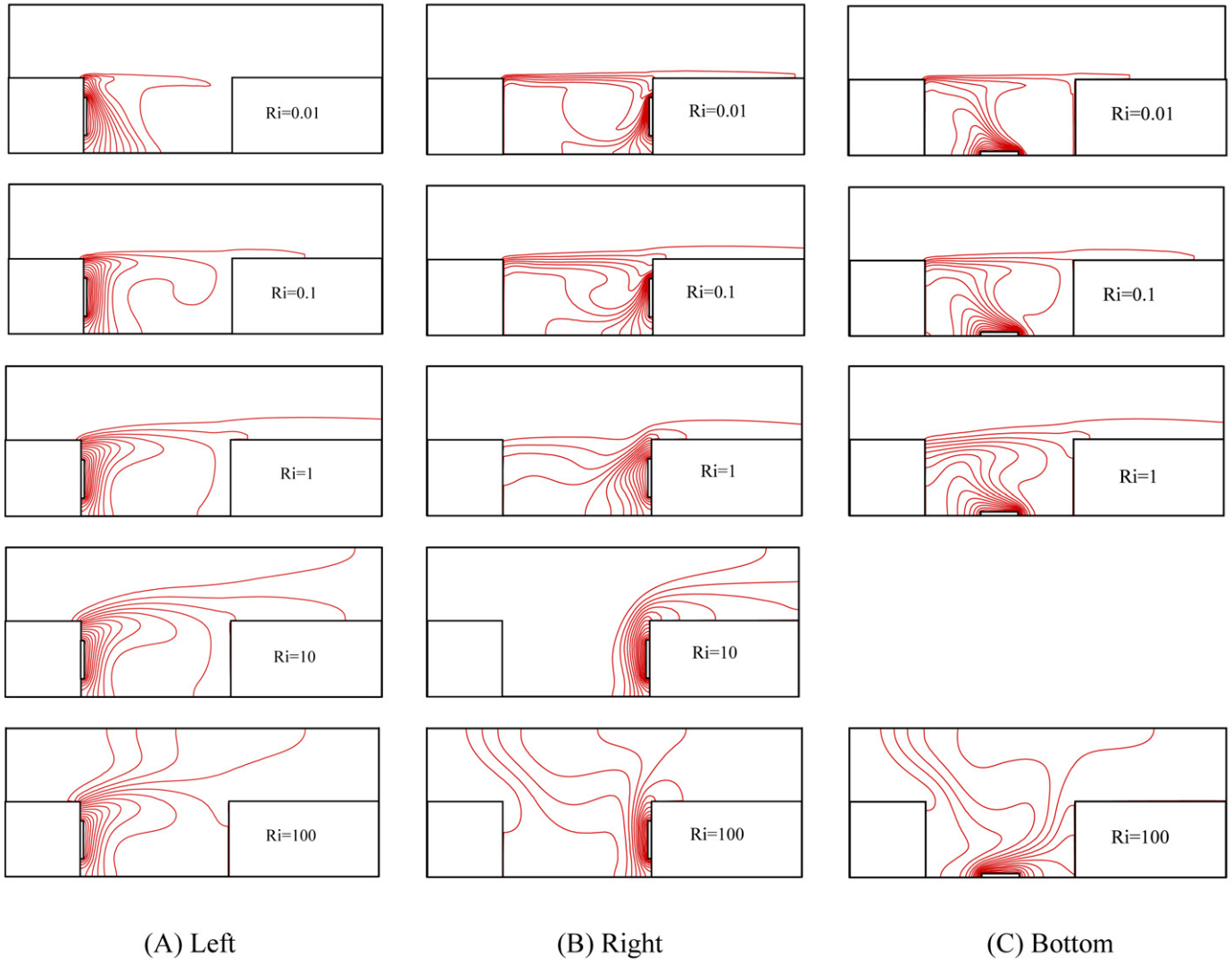

Fig. 5. Temperature patterns for different locations of the heat source and various Richardson numbers.

$\theta = 0$ and for all the walls and the exit section, adiabatic conditions ($\partial\theta/\partial X = 0$ or $\partial\theta/\partial Y = 0$) are considered. The steady-state solutions can be obtained by setting the time dependence terms to zero in the above unsteady non-dimensional equations. For the unsteady analysis, $U = 0$, $V = 0$, and $\theta = 0$ are used as the initial conditions.

To examine the required exit length of the channel, various values of Le/H are considered in the analysis. The differences for Nu, $\psi_{\min}$, $\psi_{\max}$ and θ_{fm} are found to be less than 1×10^{-3} when Le/H is set to values greater than 2. Hence, $Le/H = 2$ is used in the whole analysis. The local Nusselt number is defined as $Nu = -(\partial\theta/\partial N)_s$ and can be determined from the temperature distribution. The average Nusselt number is obtained by integrating the Nusselt number over the heat source surface area as $Nu_m = (1/s)\int_s -(\partial\theta/\partial N)_s \, \mathrm{d}s$, where s is the dimensionless total surface of the heat source being in contact with the fluid, and N is the dimensionless normal component to the surface (X or Y).

4. Numerical method

The system of governing equations (1)–(4) with the above-mentioned boundary conditions is solved through a control volume formulation of the finite difference method. The SIMPLE algorithm is used to handle the pressure-velocity coupling. The convective fluxes across the surfaces of the control volume are determined by the power law discretisation scheme described by Patankar [21]. A non-equidistant grid with a concentration of grid lines near the walls of the cavity is used in the analysis. In order to select the appropriate grid, a systematic grid independence study is carried out. A sample of the results is presented in Fig. 3 for a channel with the heat source located on the bottom wall, $Ri = 1$, $L/H = 2$ and $Le/H = 2$. A non-equidistant grid of 140×60 is found to meet the requirements of both the grid independency study and the computational time limits. For higher aspect ratios of the cavity, the number of grid points in the X direction is increased accordingly. The maximum mass residual below 10^{-7} is considered as the convergence condition.

5. Results

In order to validate the present numerical code, the steady-state solution, obtained in a two-dimensional channel with a uniform heat flux on the vertical wall of the cavity on the inflow side (left wall), is compared with the results of Manca et al. [21]. The results (Table 1) show a maximum difference of 1% for the maximum fluid temperature and a maximum difference of 1.9% for the minimum stream function.

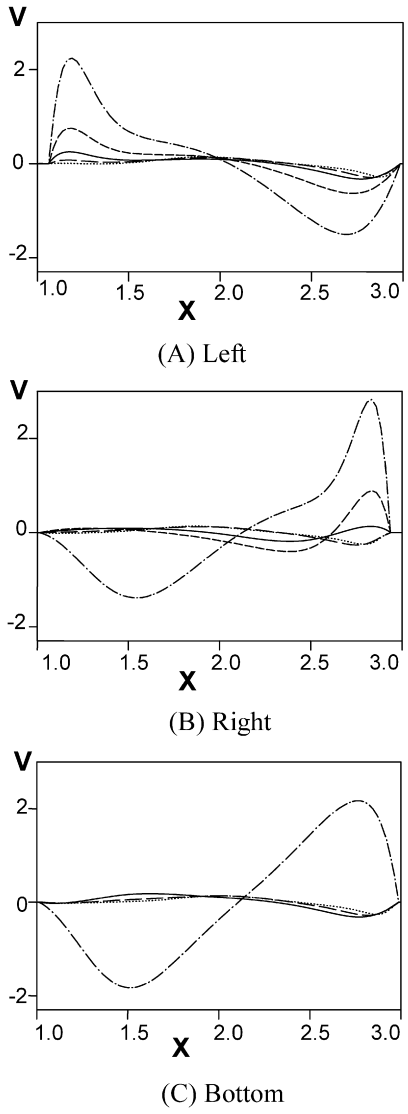

Fig. 6. Vertical component of velocity at midsection of the cavity ($Y = 0.5$). $\cdots$ $Ri = 0.01$, -- $Ri = 0.1$, — $Ri = 1$, --- $Ri = 10$, -·-· $Ri = 100$.

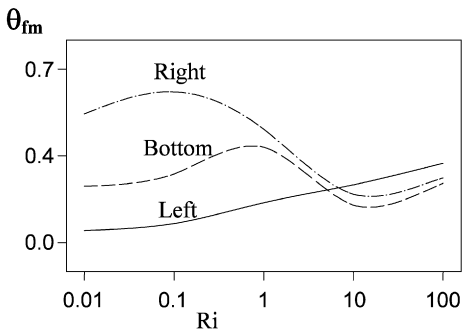

Fig. 7. Average air temperature in the cavity.

5.1. The influence of the heat source location

The flow and temperature patterns are first examined (Figs. 4 and 5) to investigate the interaction between the forced flow and the natural convection flow in the cavity for three different locations of the heat source. Fig. 4 shows that at low *Ri*, regardless of where the heat source is located, the momentum of the externally induced air flow in the channel dominates the flow field in the entire channel indicating that the circulating patterns in the cavity are mainly due to the current of forced flow not the buoyant flow. As *Ri* increases, the buoyant flow dominates the flow field and different results are obtained as the location of the heat source changes. When the heat source is located on the left wall (Fig. 4A), the circulating patterns nearly cover the whole cavity for $Ri = 100$. This can be attributed to the natural convection flow and the forced flow being in the same direction. However, when the heat source is located either on the right or the bottom wall (Figs. 4B, 4C) the externally induced air flow tends to be drawn into the cavity and the buoyancy forces generate a circulation cell in the channel above the cavity. It must be noted that for the heat source located on the bottom wall, at $Ri = 10$, the flow field experiences an oscillatory behaviour with no steady solution. That is why the results are not presented in Fig. 4C.

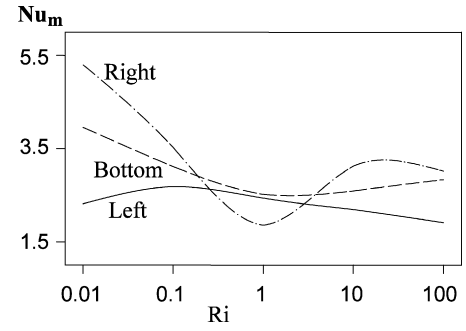

Fig. 8. Average Nusselt number.

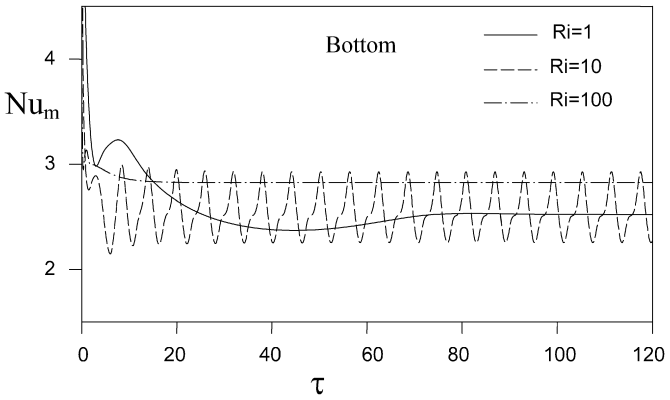

Fig. 9. Average Nusselt number versus time (heat source is located on the bottom wall of the cavity).

Fig. 5 shows that at low *Ri*, regardless of the heat source location, the temperature distribution is rather uniform in the channel except in the vicinity of the heat source. As *Ri* increases, the temperature contours move slightly inside the channel showing a gradual growth of the high temperature zones due to the domination of natural convection effects.

Fig. 6 presents the vertical velocity profiles across the horizontal midsection of the cavity ($Y = 0.5$) for different values of *Ri* and various locations of the heat source. The results show that at low *Ri*, the velocity profile does not significantly vary across the midsection indicating a weak circulation zone in the cavity. As *Ri* increases, the flow field is characterised by a stronger circulation cell and higher magnitude of vertical velocity. It must also be noted that when the heat source is located on the bottom or right wall, the direction of the vertical velocity indicates an anticlockwise circulation, whereas, when the heat source is located on the left wall, the circulation is clockwise.

Fig. 7 shows that at low *Ri*, placing the heat source on the left wall of the cavity results in a lower average air temperature in the

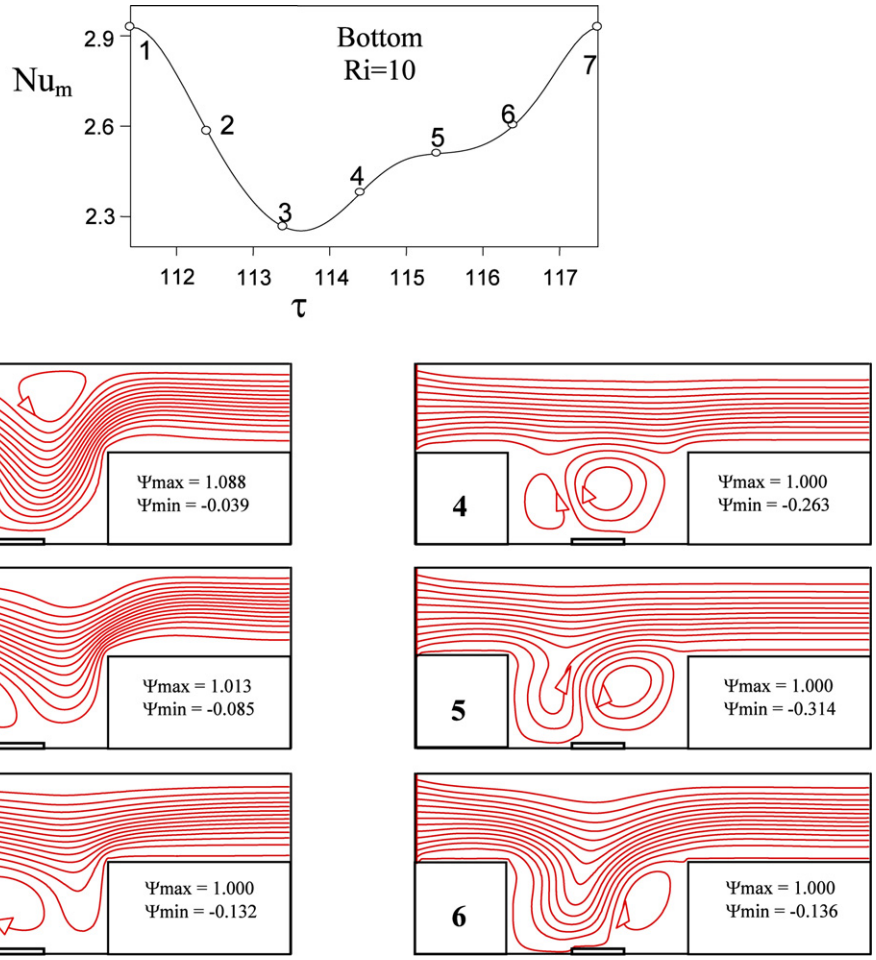

Fig. 10. The flow patterns in a complete periodic cycle ($Ri = 10$).

entire cavity. This can be attributed to the forced and natural convection flows being in the same direction and assisting each other. When the heat source is located on the left wall, as Ri increases, the average temperature increases. This is because the momentum of the relatively low temperature forced flow entering the cavity decreases. When the heat source is located on the bottom or right wall of the cavity, lower temperatures are observed, as Ri increases. This behaviour is a result of the forced flow being drawn into the cavity, lowering the temperature of the air flow, as suggested by Fig. 4.

Fig. 8 shows the variation of average Nusselt number (Nu_m) with Ri for three different locations of the heat source. In general, the lowest Nu_m corresponds to the heat source on the left, whereas, the highest Nu_m is achieved for the heat source on the right, except for $Ri = 1$. For the heat source on the left, Nusselt number initially increases until it reaches its maximum at $Ri = 0.1$ and then decreases. The interaction of the natural convection flow and the forced flow in the cavity accounts for this variation. For the heat source on the right or bottom wall, Nu_m first decreases as there is no penetration of induced forced flow in the cavity. Nu_m reaches its minimum at about $Ri = 1$ and then increases. The reason is that even though the externally induced air flow is weaker, it starts penetrating into the cavity at higher Ri.

As mentioned earlier, at $Ri = 10$ for the heat source on the bottom wall, fluctuating results are observed similar to the one noticed by Manca et al. [15], Papanicolaou and Jaluria [22] and D'Orazio et al. [23]. They argued that the instability in the physical system can explain the fluctuating results at particular geometries and flow field conditions. Other researchers [24–26] also found the fluctuating results in the closed and opened cavities and discussed that the Hopf bifurcations lead to oscillating flows. In the present analysis, the examination of the heat removal process for the heat source on the bottom wall and $Ri = 10$ is based on solving the unsteady equations using the time step of $\Delta\tau = 0.1$. This was selected after a thorough examination of various time steps on the results. Periodic solutions for the flow parameters are detected in the results. As an example of the results of unsteady governing equations, Fig. 9 presents the variation of Nu_m with time for $Ri = 1$, 10 and 100. It can be seen that steady-state results can be obtained for $Ri = 1$ and 100, whereas, for $Ri = 10$, Nu_m decreases with time until it reaches an asymptotic periodic zone with a train of identical pulses. Once the asymptote region is reached it can be seen that the value of Nu_m fluctuates in a periodic manner. It must be noted that the steady-state values of θ_{fm} and Nu_m presented in Figs. 7 and 8, are obtained from the average of maximum and minimum values of θ_{fm} and Nu_m in the asymptotic periodic zone.

The periodic cycle is clearly illustrated in Fig. 10. At the start of the cycle (state 1), the majority of the induced flow penetrates into the cavity and flows over the heat source, generating a circulation cell above the cavity. As time passes (state 2), the top circulation cell disappears, however another circulation cell is generated near the left wall. This circulation cell is then split into two cells (states 3 and 4) one of which merges with the forced flow (state 5), while the other one becomes gradually weaker (state 6). Eventually, at the end of the cycle (state 7), similar behaviour of the flow field as observed at the start can be seen.

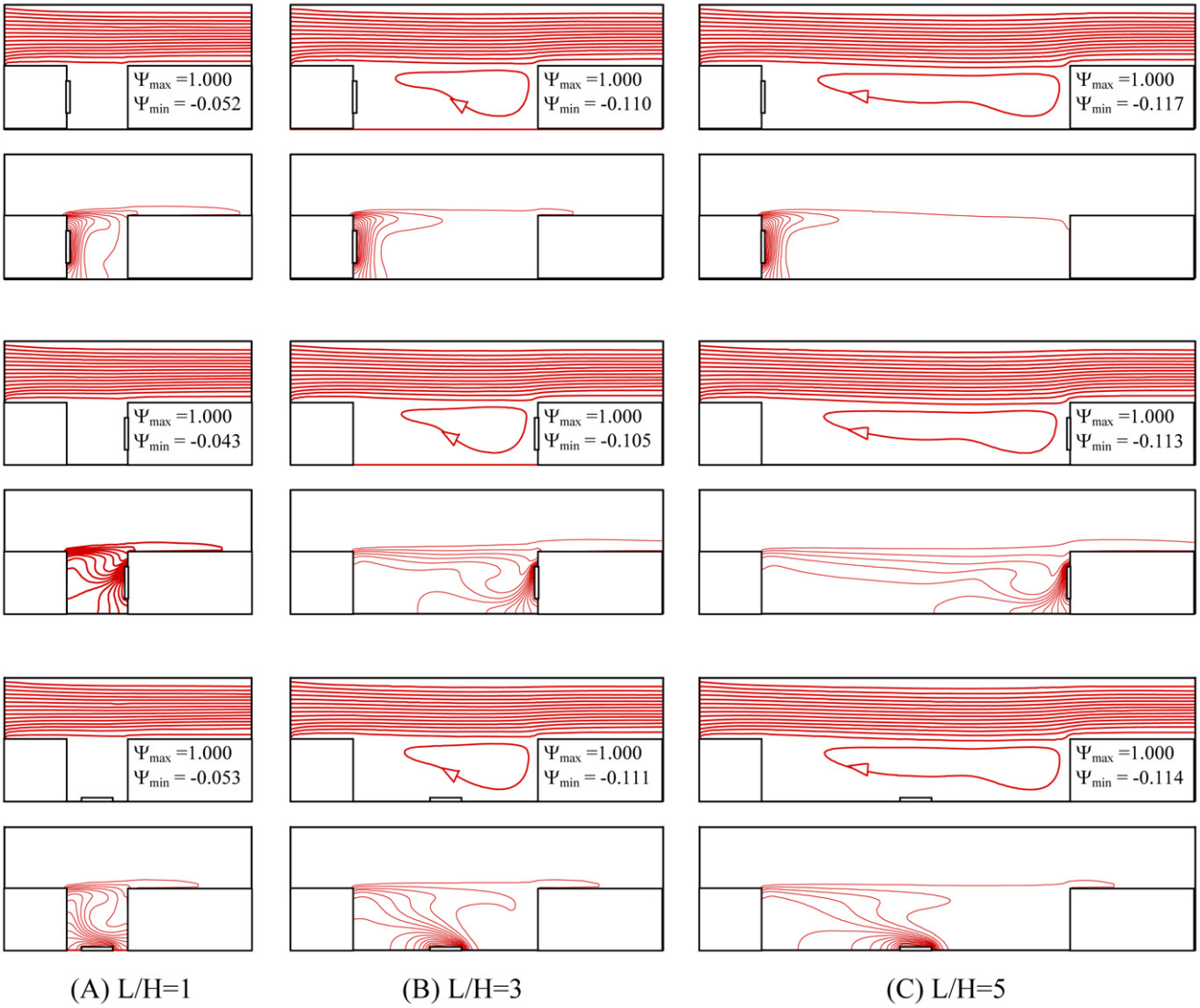

Fig. 11. The flow and temperature patterns for various aspect ratios of the cavity ($Ri = 0.1$).

5.2. The effects of aspect ratio of the cavity

For three different values of aspect ratio ($L/H = 1$, 3 and 5), Figs. 11 and 12 present the flow and temperature fields for $Ri = 0.1$ and $Ri = 100$ respectively. At $Ri = 0.1$, regardless of the aspect ratio, the location of the heat source does not significantly change the flow field within the cavity. However, at $Ri = 100$, there is a significant change in the flow and temperature patterns as the location of the heat source changes. For all values of aspect ratio, when the heat source is located on the bottom or right wall, the forced flow penetrates into the cavity creating an anticlockwise circulation cell which becomes larger as the aspect ratio increases. When the heat source is located on the left wall, as the aspect ratio increases, the clockwise circulation cell in the cavity gradually expands and moves towards the left wall.

The influence of the cavity aspect ratio (L/H) on the average air temperature in the cavity (θ_{fm}) is shown in Fig. 13. At $Ri = 0.1$ (Fig. 13A) and for all values of $L/H \geqslant 1$, θ_{fm} increases as the heat source is shifted from the left to the bottom and then to the right. This is because the length of the air travelling path increases before being able to exchange heat with the low temperature mainstream in the channel. In addition, for the three locations of the heat source, as L/H increases, θ_{fm}, decreases. This can be attributed to the increase in the penetration of the externally induced flow into the cavity as the width of the cavity increases. At $Ri = 100$ (Fig. 13B), when the heat source is located on the left wall, the circulation cells intensify inside the cavity while there is no external air flow penetration. This mechanism associates with a slightly higher average air temperature as opposed to the other two heating modes, where the externally induced air flow penetrates into the cavity, reducing the average air temperature. As L/H increases, more flow penetration into the cavity (see Fig. 12) results in further reduction of the average air temperature. This trend can be seen for all locations of the heat source.

Fig. 14 shows the variation of Nu_m with respect to L/H. At $Ri = 0.1$ (Fig. 14A) and for the three different locations of the heat source, Nu_m increases with L/H. This is because of more penetration of forced flow into the cavity and higher circulating flow intensity at higher aspect ratios. For $Ri = 100$ (Fig. 14B) and $L/H < 2$, when the heat source moves from the left, to the bottom and then to the right of the cavity, the rate of heat transfer increases because the amount of forced flow entering the cavity increases. For $L/H > 2$, when the heat source is on the right or bottom wall, the low temperature forced flow enters the cavity, helping the heat transfer from the heat source. Therefore, the rate of heat transfer

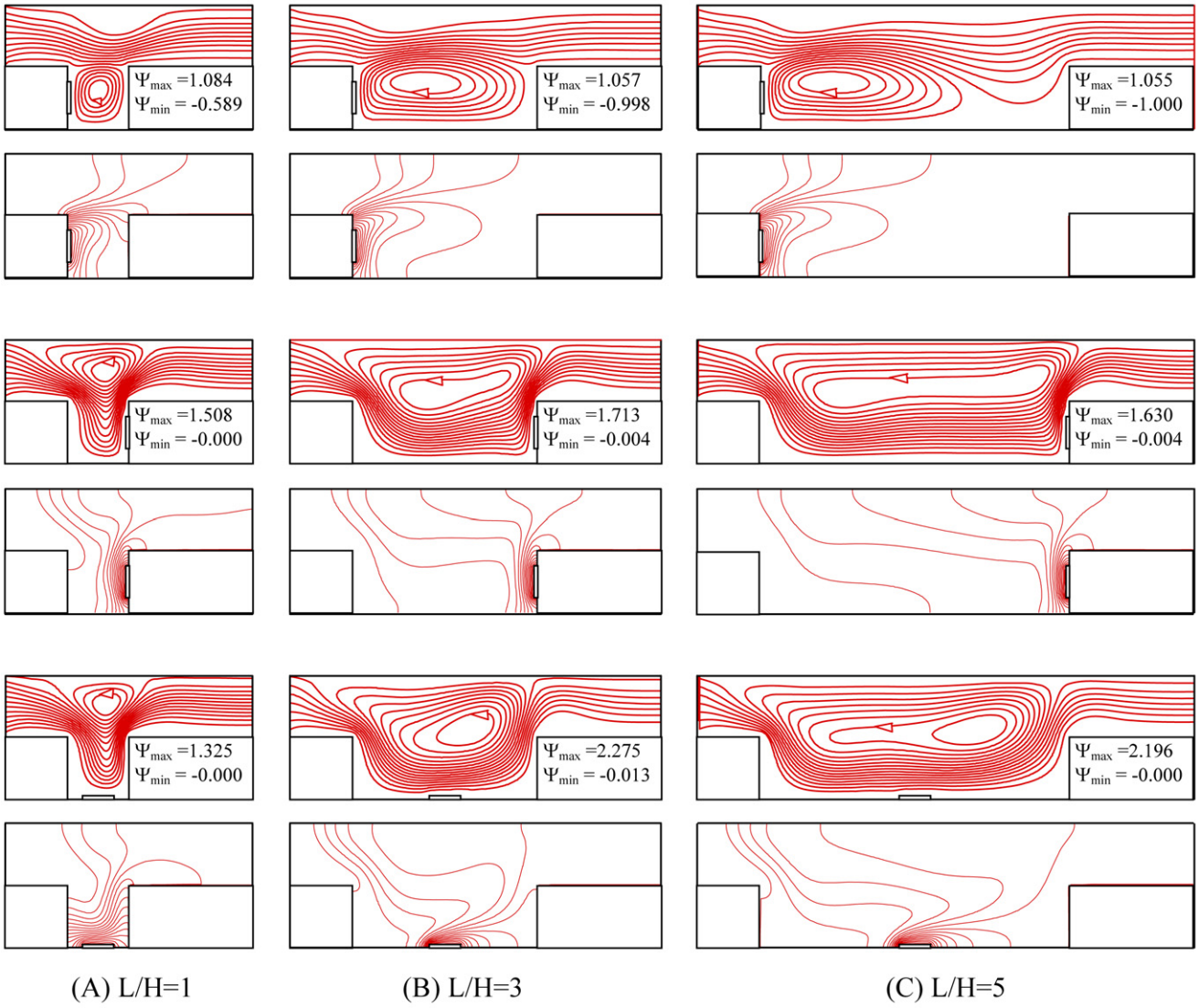

Fig. 12. The flow and temperature patterns for various aspect ratios of the cavity ($Ri = 100$).

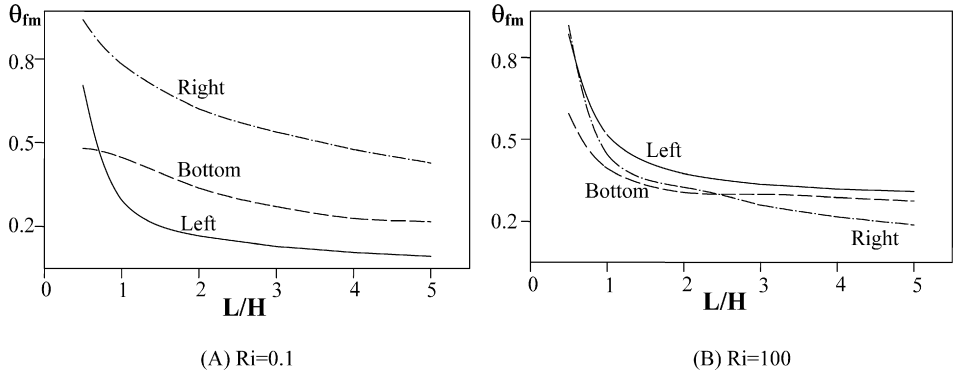

(A) Ri=0.1 (B) Ri=100

Fig. 13. Average temperature versus the cavity aspect ratio.

is almost the same and still higher than that for the heat source located on the left wall.

6. Concluding remarks

The problem of mixed convection heat transfer in a horizontal channel with an open cavity has been studied numerically. Three different scenarios which relate to the location of a discrete heat source on the left, bottom or right wall of the cavity have been considered. For every scenario, the results of the flow and temperature fields and the heat transfer rate have been presented for different values of Richardson numbers and aspect ratios of the cavity. The results of the numerical analysis lead to the following conclusions:

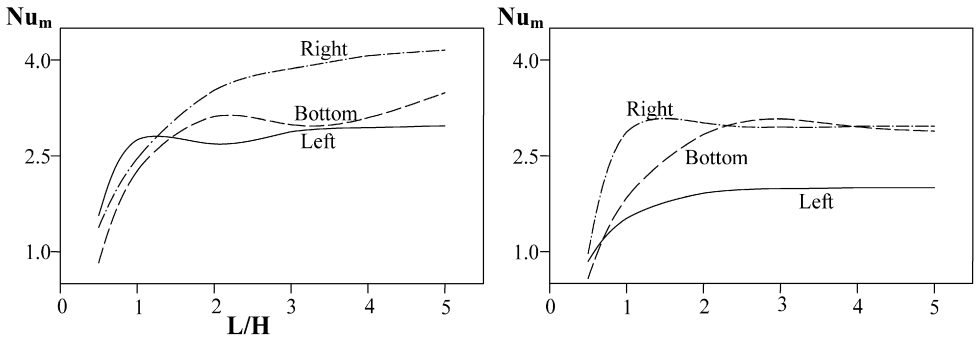

Fig. 14. Average Nusselt number versus the cavity aspect ratio.

- At low *Ri*, the momentum of the externally induced air flow in the channel dominates the flow in the entire channel and the buoyancy forces in the cavity are overwhelmed by the effects of the forced flow. For all values of the cavity aspect ratio and locations of the heat source, slight differences can be observed in the flow field. For the cavity aspect ratio above one, both the average temperature and the heat transfer rate increase as the heat source moves from the left, to the bottom and then to the right.
- At high *Ri*, heat transfer enhancement is obtained more due to the development of buoyancy induced flow. The flow field behaves differently when the heat source is located on different walls of the cavity. More of the low temperature main flow is drawn into the cavity, lowering the air average temperature of air when the heat source is on the bottom or on the right wall. This can be seen at all cavity aspect ratios. For the cavity aspect ratio above two, when the heat source is located on the right, a better cooling performance is achieved in comparison to the other two cases.
- For all different locations of the heat source in the cavity, as the cavity aspect ratio increases, an initial decrease in the average temperature and an increase in the heat transfer rate can be observed for low aspect ratios of the cavity; however this trend stabilises at higher values of aspect ratio.
- At $Ri = 10$, $L/H = 2$ and for the heat source on the bottom wall, the results undergo a fluctuating phase. The flow field within the cavity experiences the formation of a vortex oscillate, breaking up to two zones and then mixing with the mainstream flow in the channel.
- The results of this study suggest several guidelines for the thermal design of electronic packages where the geometry of electronic devices and the arrangement of electronic components are of interest.

References

[1] F.P. Incropera, Convection heat transfer in electronic equipment, Journal of Heat Transfer 110 (4) (1988) 1097–1111.
[2] G.P. Peterson, A. Ortega, Thermal control of electronic equipment and devices, Advances in Heat Transfer 20 (1990) 181–314.
[3] T.J. Young, K. Vafai, Convective flow and heat transfer in a channel containing multiple heated obstacles, International Journal of Heat and Mass Transfer 41 (1998) 3279–3298.
[4] A.K. da Silva, G. Lorenzini, A. Bejan, Distribution of heat sources in vertical open channels with natural convection, International Journal of Heat and Mass Transfer 48 (8) (2005) 1462–1469.
[5] Y.P. Cheng, T.S. Lee, H.T. Low, Numerical analysis of mixed convection in three-dimensional rectangular channel with flush-mounted heat sources based on field synergy principle, International Journal for Numerical Methods in Fluids 52 (9) (2006) 987–1003.
[6] A. Dogan, M. Sivrioglu, S. Baskaya, Investigation of mixed convection heat transfer in a horizontal channel with discrete heat sources at the top and at the bottom, International Journal of Heat and Mass Transfer 49 (15–16) (2006) 2652–2662.
[7] M. Hasnaoui, E. Bilgen, P. Vasseur, Natural convection above an array of open cavities heated from below, Numerical Heat Transfer, Part A 18 (1990) 463–482.
[8] G.F. Jones, J. Cai, Analysis of a transient asymmetrically heated/cooled open thermosyphon, Journal of Heat Transfer 115 (1993) 621–630.
[9] R.A. Showole, J.D. Tarasuk, Experimental and numerical studies of natural convection with flow separation in upward-facing inclined open cavities, Journal of Heat Transfer 115 (3) (1993) 592–605.
[10] S.W. Chang, S.F. Chiou, L.M. Su, T.L. Yang, Free connective heat transfer in tilted longitudinal open cavity, Heat Transfer Engineering 26 (10) (2005) 46–64.
[11] M. El Alami, M. Najam, E. Semma, A. Oubarra, F. Penot, Electronic components cooling by natural convection in horizontal channel with slots, Energy Conversion and Management 46 (17) (2005) 2762–2772.
[12] K. Vafai, C.P. Desai, S.V. Iyer, M.P. Dyko, Buoyancy induced convection in a narrow open-ended annulus, ASME Journal of Heat Transfer 119 (3) (1997) 483–494.
[13] T. Fusegi, Numerical study of convective heat transfer from periodic open cavities in a channel with oscillatory throughflow, International Journal of Heat and Fluid Flow 18 (4) (1997) 376–383.
[14] K. Khanafer, K. Vafai, Buoyancy-driven flow and heat transfer in open-ended enclosures: elimination of the extended boundaries, International Journal of Heat and Mass Transfer 43 (22) (2000) 4087–4100.
[15] O. Manca, S. Nardini, K. Khanafer, K. Vafai, Effect of heated wall position on mixed convection in a channel with an open cavity, Journal of Numerical Heat Transfer 43 (3) (2003) 259–282.
[16] N.M. Brown, F.C. Lai, Correlations for combined heat and mass transfer from an open cavity in a horizontal channel, International Communications in Heat and Mass Transfer 32 (8) (2005) 1000–1008.
[17] J.C. Leong, N.M. Brown, F.C. Lai, Mixed convection from an open cavity in a horizontal channel, International Communications in Heat and Mass Transfer 32 (5) (2005) 583–592.
[18] O. Manca, S. Nardini, K. Vafai, Experimental investigation of mixed convection in a channel with an open cavity, Experimental Heat Transfer 19 (1) (2006) 53–68.
[19] P.H. Oosthuizen, J.T. Paul, Mixed convective heat transfer in a cavity, in: AME-HTD, vol. 42, 1985, pp. 159–169.
[20] J.P. Simoneau, C. Inard, F. Allard, Numerical approach of interaction between an injection and laminar natural convection in a thermally driven cavity, in: Natural Convection in Enclosures, ASME HTD, vol. 99, 1988, pp. 45–51.
[21] S.V. Patankar, Numerical Heat Transfer and Fluid Flow, Hemisphere Publishing Corp, Washington, DC, 1980.
[22] E. Papanicolaou, Y. Jaluria, Transition to a periodic regime in mixed convection in a square cavity, Journal of Fluid Mechanic 239 (1992) 489–509.
[23] M.C. D'Orazio, C. Cianfrini, M. Corcione, Rayleigh–Bénard convection in tall rectangular enclosures, International Journal of Thermal Sciences 43 (2) (2004) 135–144.
[24] C.C. Jahnke, V. Subramanyan, D.T. Valentine, On the convection in an enclosed container with unstable side wall temperature distributions, International Journal of Heat and Mass Transfer 41 (1998) 2307–2320.
[25] A. Javam, S.W. Armfield, Stability and transition of stratified natural convection flow in open cavities, Journal of Fluid Mechanics 445 (2001) 285–303.
[26] Y. Li, P. Xu, H. Qian, Q.H. Deng, J. Wu, Flow bifurcation due to opposing buoyancy in two vertically connected open cavities, International Journal of Heat and Mass Transfer 49 (19–20) (2006) 3298–3312.